A Joint Experimental and Computational Study of the Negative Ion Photoelectron Spectroscopy of the 1-Phospha-2,3,4-Triazolate Anion, $HCPN_3$#

A Joint Experimental and Computational Study of the Negative Ion Photoelectron Spectroscopy of the 1-Phospha-2,3,4-triazolate...

Article *in* The Journal of Physical Chemistry A · July 2016

DOI: 10.1021/acs.jpca.6b06343

7 authors, including:

Gao-Lei Hou
Pacific Northwest National Laboratory
65 PUBLICATIONS **143** CITATIONS
SEE PROFILE

Xue-Bin Wang
Pacific Northwest National Laboratory
213 PUBLICATIONS **6,153** CITATIONS
SEE PROFILE

THE JOURNAL OF PHYSICAL CHEMISTRY A

Article

pubs.acs.org/JPCA

A Joint Experimental and Computational Study of the Negative Ion Photoelectron Spectroscopy of the 1-Phospha-2,3,4-triazolate Anion, $HCPN_3^-$

Gao-Lei Hou,[†] Bo Chen,[*,¶] Wesley J. Transue,[§] David A. Hrovat,[‡] Christopher C. Cummins,[*,§] Weston Thatcher Borden,[*,‡] and Xue-Bin Wang[*,†]

[†]Physical Sciences Division, Pacific Northwest National Laboratory, P.O. Box 999, MS K8-88, Richland, Washington 99352, United States

[¶]Department of Chemistry and Chemical Biology, Baker Laboratory, Cornell University, Ithaca, New York 14853, United States

[‡]Department of Chemistry and the Center for Advanced Scientific Computing and Modeling, University of North Texas, 1155 Union Circle, #305070, Denton, Texas 76203-5017, United States

[§]Department of Chemistry, Massachusetts Institute of Technology, Cambridge, Massachusetts 02139, United States

Supporting Information

ABSTRACT: We report here the results of a combined experimental and computational study of the negative ion photoelectron spectroscopy (NIPES) of the recently synthesized, planar, aromatic, $HCPN_3^-$ ion. The adiabatic electron detachment energy of $HCPN_3^-$ (electron affinity of $HCPN_3^{\bullet}$) was measured to be 3.555 ± 0.010 eV, a value that is intermediate between the electron detachment energies of the closely related $(CH)_2N_3^-$ and $P_2N_3^-$ ions. High level electronic structure calculations and Franck−Condon factor (FCF) simulations reveal that transitions from the ground state of the anion to two nearly degenerate, low-lying, electronic states, of the neutral $HCPN_3^{\bullet}$ radical are responsible for the congested peaks at low binding energies in the NIPE spectrum. The best fit of the simulated NIPE spectrum to the experimental spectrum indicates that the ground state of $HCPN_3^{\bullet}$ is a 5π-electron $^2A''$ π radical state, with a 6π-electron, $^2A'$, σ radical state being at most 1.0 kcal/mol higher in energy.

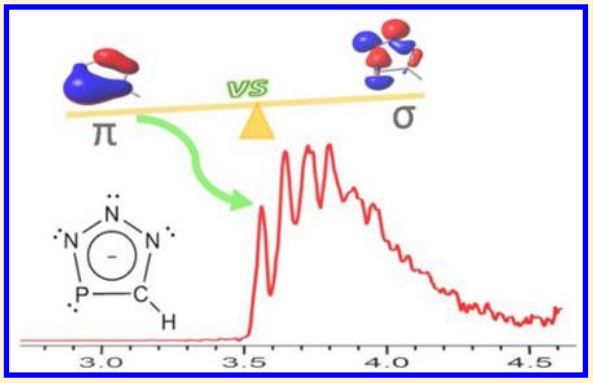

1. INTRODUCTION

Until recently, the *cyclo*-pentaphosphorus anion (P_5^-) represented the only all-pnictogen analogue of cyclopentadienide anion ($C_5H_5^-$)[1−6] that could be synthesized and isolated in bulk quantities.[7−9] Although the *cyclo*-pentazolate anion (N_5^-) was observed in the gas phase more than a decade ago[10] and has been calculated to be a stable species,[11] attempts to synthesize it in large quantities have, at least thus far, been futile.[12] Consequently, the recent synthesis of $P_2N_3^-$ represents important progress in the study of all-pnictogen analogues of $C_5H_5^-$.[13−17]

Formal replacement of both phosphorus atoms in $P_2N_3^-$ by CH groups yields the 1,2,3-triazolide anion, $(CH)_2N_3^-$ (Figure 1). In 2008, Lineberger and co-workers reported the 335 nm negative ion photoelectron (NIPE) imaging spectrum of $(CH)_2N_3^-$ and measured the adiabatic electron detachment energy [i.e., ionization energy (IE)] of this anion.[18] Later, Dillon et al. simulated the NIPE spectrum of $(CH)_2N_3^-$ using a quasidiabatic Hamiltonian to study the vibronic energy levels of the neutral 1,2,3-triazolyl radical $(CH)_2N_3^{\bullet}$.[19]

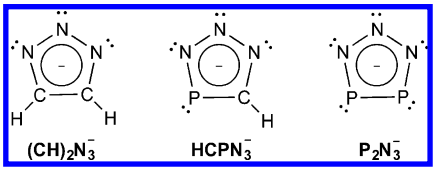

Figure 1. Schematic depictions of the $(CH)_{2-n}P_nN_3^-$ series (n = 0−2).

The IE of $(CH)_2N_3^-$ [3.447(4) eV][18] is significantly larger than that of $C_5H_5^-$ [IE = 1.808(6) eV],[2] but only slightly smaller than that of $P_2N_3^-$ [IE = 3.765(10) eV].[20] Comparisons of the $(CH)_2N_3$ anion and radical with the previously studied $(CH)_4N$[21] and $(CH)_3N_2$[22,23] species found that substitution of each CH group in $C_5H_5^{-/\bullet}$ by an isoelectronic N atom has a significant effect on the chemistry and thermodynamic properties, such as the C−H bond dissociation energies and gas-phase acidities, of these three nitrogen-containing analogues of $C_5H_5^-$.

Received: June 22, 2016
Revised: July 19, 2016

DOI: 10.1021/acs.jpca.6b06343
J. Phys. Chem. A XXXX, XXX, XXX−XXX

In a recent Communication, Transue et al. reported the synthesis of the 1-phospha-2,3,4-triazolate anion, $HCPN_3^-$.[24] This anion can be viewed as the $n = 1$ member of the series, $(CH)_{2-n}P_nN_3^-$ ($n = 0-2$). Nucleus-independent chemical shift (NICS) and quantum theory of atoms in molecules (QTAIM) calculations showed that $HCPN_3^-$ is aromatic, with its aromaticity being intermediate between that of the $n = 0$ $[(CH)_2N_3^-]$ and the $n = 2$ $(P_2N_3^-)$ members of this series.

In this paper we report the detailed results of NIPE spectroscopy and electronic structure calculations on $HCPN_3^-$ and the neutral radical formed from it. Our experimental and computational results are compared with those for $(CH)_2N_3^-$ [18] and $P_2N_3^-$ [20] as well as the neutral radicals formed from them.

2. EXPERIMENTAL METHODS

The NIPES experiment was performed with an apparatus consisting of an electrospray ionization source (ESI), a cryogenic ion trap, and a magnetic-bottle time-of-flight (TOF) photoelectron spectrometer.[25] An acetonitrile solution of the tetrabutylammonium (TBA) salt of $HCPN_3^-$, whose synthesis was recently reported by Transue et al.,[24] was prepared in the glovebox under an N_2 atmosphere. The solution was transferred immediately into the electrospray ionization source, which was purged with N_2, in order to minimize the O_2 and moisture content of the solution.

The electrospray ionization conditions were optimized, to make sure there was only one dominant peak at $m/z = 86$ (i.e., the mass of $HCPN_3^-$) in the mass spectrum (Figure S1 in the Supporting Information). The anions generated by ESI were guided by quadrupole ion guides into an ion trap, where they were accumulated and cooled for 20−100 ms by collisions with cold buffer gas at 20 K, before being transferred into the extraction zone of a TOF mass spectrometer. The cooling of the anions to 20 K eliminated the possibility of the appearance of peaks in the NIPE spectra due to hot bands.

The $HCPN_3^-$ anions were then mass selected, and maximally decelerated before being photodetached with 266 nm (4.661 eV) photons from a Nd:YAG laser or with 193 nm (6.424 eV) photons from a ArF excimer laser. Both lasers were operated at a 20 Hz repetition rate, with the ion beam off at alternating laser shots, in order to enable shot-to-shot background subtraction to be carried out.

Photoelectrons were collected with *ca.* 100% efficiency with the magnetic bottle and analyzed in a 5.2 m long electron flight tube. The recorded TOF photoelectron spectrum was converted into an electron kinetic energy spectrum by calibration with the known NIPE spectra of I^-, $OsCl_6^{2-}$, and/or $Cu(CN)_2^-$. The electron binding energy spectrum was obtained by subtracting the electron kinetic energy spectrum from the energy of the detaching photons. The energy resolution was about 2%, i.e., ~20 meV for 1 eV kinetic energy electrons.

3. COMPUTATIONAL DETAILS

In order to help analyze the NIPE spectra of $HCPN_3^-$, three different types of electronic structure calculations were performed: B3LYP density functional theory (DFT) calculations,[26] CASPT2 many body perturbation methods,[27] and CCSD(T) coupled-cluster *ab initio* calculations.[28,29] The aug-cc-pVTZ basis set[30,31] was employed in all three types of calculations, although the smaller aug-cc-pVDZ basis set[30,31] was used for some of the initial CASPT2 calculations.

A (14/9)CASSCF active space was used for $HCPN_3^-$ in the CASPT2 calculations. The (14/9) active space consisted of four, highest, doubly occupied σ MOs, which are mainly in-plane, lone pair orbitals on the P and three N atoms, plus all five valence π and π^* MOs, three of which are doubly occupied in the lowest electronic configuration. The active space used for $HCPN_3^{\bullet}$ was (13/9), since the radical has one less active electron than the anion.

The B3LYP geometry optimizations and harmonic vibrational analyses were performed using the Gaussian09 suite of programs.[32] The CASPT2 calculations were carried out with the Molcas program (version 8).[33] The CCSD(T) geometry optimizations and vibrational analyses were performed using the Molpro 10 program.[34] The program ezSpectrum[35] was used to compute the Franck−Condon factors (FCFs) that were necessary in order to simulate the vibrational progressions in the NIPE spectra of $HCPN_3^-$.

A temperature of 20 K was used in the simulations of the NIPE spectra. As expected, no vibrational hot bands were seen in the simulations. In carrying out the simulations, the imaginary frequencies of some vibrations in the electronic states of the radical were treated as real frequencies; but the FCFs for these modes were calculated to be zero.

4. RESULTS AND DISCUSSION

4.1. The NIPE Spectra of $HCPN_3^-$. Figure 2 presents the 20 K NIPE spectra of $HCPN_3^-$ at 266 and 193 nm. It can be seen that the 193 nm NIPE spectrum contains three main broad spectral features in the electron binding energy ranges of EBE = 3.5−4.4, 4.5−5.2, and 5.4−5.9 eV.

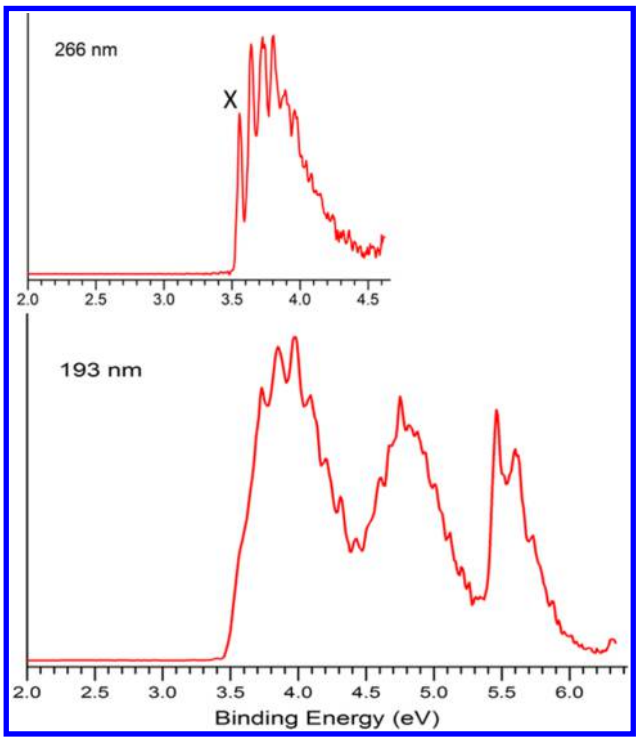

Figure 2. The 20 K NIPE spectra of $HCPN_3^-$ at 266 (4.661 eV) and 193 nm (6.424 eV), respectively. The origin of the band for what appears to be the first electronic state of $HCPN_3^{\bullet}$ is labeled X in the 266 nm spectrum.

DOI: 10.1021/acs.jpca.6b06343
J. Phys. Chem. A XXXX, XXX, XXX−XXX

Table 1. Comparison of the X-ray Structure of $HCPN_3^-$ in [TAS][$HCPN_3$] Solid Salt with the Calculated Structures at Three Levels of Theory[a]

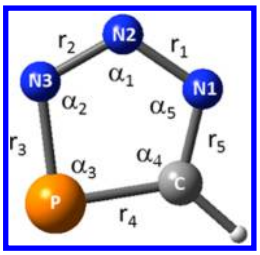

	r_1	r_2	r_3	r_4	r_5	α_1	α_2	α_3	α_4	α_5
X-ray structure	1.347	1.328	1.684	1.722	1.340	114.9	112.0	89.5	112.0	111.6
B3LYP/aug-cc-pVTZ	1.344	1.310	1.705	1.742	1.338	115.5	112.4	88.4	112.1	111.6
(14/9)CASPT2/aug-cc-pVTZ	1.334	1.339	1.691	1.729	1.359	115.5	111.7	89.6	111.7	111.6
CCSD(T)/aug-cc-pVTZ	1.351	1.324	1.709	1.743	1.349	115.5	112.2	88.6	112.4	111.3

[a]Bond distances (r_1–r_5) are in angstroms (Å) and bond angles (α_1–α_5) are in degrees (°).

In the 266 nm spectrum of $HCPN_3^-$, the intrinsic energy resolution of the instrument is better than in the 193 nm spectrum, due to the reduced detachment photon energy. As a result, the broad spectral features in the EBE range of 3.5–4.4 eV that is observed in the 193 nm spectrum become narrower and better resolved. However, the 266 nm spectrum still contains at least six closely spaced peaks. As in our recent NIPES study of $P_2N_3^-$,[20] these closely spaced peaks suggest that this region of the spectrum may contain transitions to more than one state of the $HCPN_3^•$ radical and the vibrational progressions that are associated with these transitions. The adiabatic IE of $HCPN_3^-$ (i.e., the electron affinity (EA) of $HCPN_3^•$) is determined from the 0–0 transition (X) in the 266 nm NIPE spectrum in Figure 2 to be EA = 3.555 ± 0.010 eV.

The value EA = 3.555 ± 0.010 eV of $HCPN_3^•$ is only slightly smaller than that of $P_2N_3^•$, which was recently measured to have EA = 3.765 ± 0.010 eV;[20] but the EA of $HCPN_3^•$ is slightly larger than that of $(CH)_2N_3^•$, which was previously measured by Lineberger and co-workers to be 3.447 ± 0.004 eV,[18] and which we remeasured as EA = 3.445 ± 0.010 eV. (See Figure S2 in the Supporting Information.)

The similar EA values for the n = 0–2 members of the $(CH)_{2-n}P_nN_3$ series of molecules may be viewed as a consequence of the fact that carbon and phosphorus have very similar electronegativities. However, the electronegativity of nitrogen is substantially larger than those of both carbon and phosphorus. Therefore, the presence of three nitrogen atoms in each of the members of this series is the reason why all of these EA values are much larger than that of $C_5H_5^•$, which has EA = 1.808 ± 0.006 eV.[2]

4.2. The Electronic Structures of $HCPN_3^-$ and $HCPN_3^•$.

In order to help interpret the NIPE spectra of $HCPN_3^-$, we carried out electronic structure calculations on both the $HCPN_3^-$ anion and the neutral $HCPN_3^•$ radical. Table 1 shows the comparison of the optimized geometries of $HCPN_3^-$, calculated at B3LYP/aug-cc-pVTZ, (14/9)CASPT2/aug-cc-pVTZ, and CCSD(T)/aug-cc-pVTZ levels of theory, with the X-ray structure in the solid tris(dimethylamino)sulfonium (TAS) salt.[24] The calculated bond lengths and bond angles are respectively within 0.021 Å and 1.1° of those determined by X-ray diffraction. This good agreement is indicative of the accuracy of all three theoretical methods employed in this work, at least for providing optimized geometries.

Figure 3 shows the eight highest occupied molecular orbitals (HOMOs) and the two virtual MOs in the lowest electronic configuration of $HCPN_3^-$. Five of the eight occupied MOs in Figure 3 are σ MOs; the other three HOMOs and the two virtual MOs are π MOs. The σ MOs are mainly composed of in-plane lone pair atomic orbitals (AOs) on P and N, with contributions from the σ orbitals of the ring bonds and the

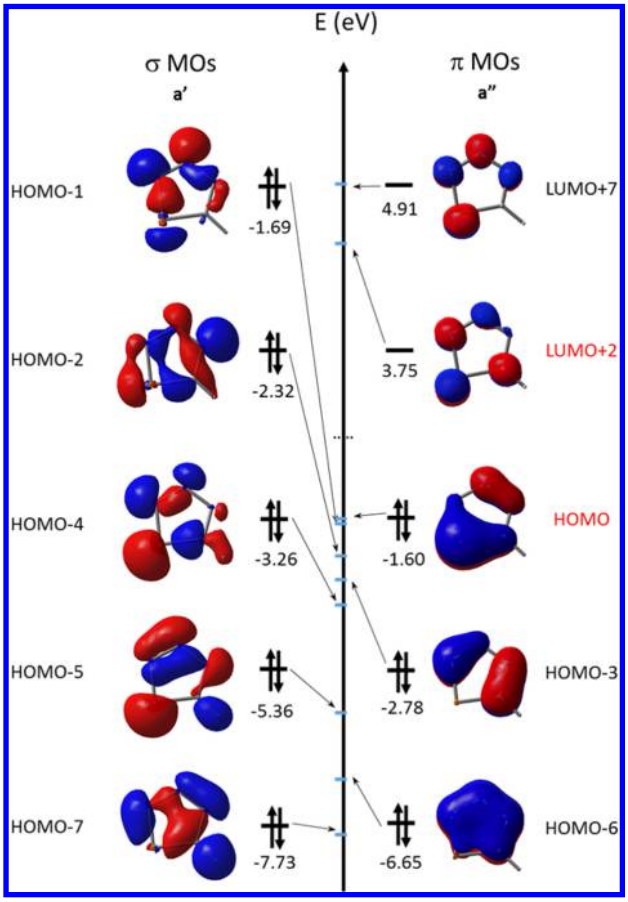

Figure 3. Eight highest occupied molecular orbitals (HOMOs) and two lowest unoccupied molecular orbitals (LUMOs) of $HCPN_3^-$ at a C_s geometry, and their orbital energies (in eV), calculated at the B3LYP/aug-cc-pVTZ level of theory. Of the virtual MOs, only the valence π^* MOs (LUMO+2 and LUMO+7) are shown. The other low-lying virtual MOs, for example, the LUMO (2.80 eV) and the LUMO+1 (3.50 eV), are Rydberg MOs, formed from diffuse functions in the aug-cc-pVTZ basis set. The Rydberg MOs are not shown here.

DOI: 10.1021/acs.jpca.6b06343
J. Phys. Chem. A XXXX, XXX, XXX–XXX

Table 2. Energies, with Zero-Point Energy (ZPE) Corrections in Parentheses, of the ^{2}A″, ^{2}A′, 2^{2}A′, and 2^{2}A″ States of $HCPN_3^•$, Relative to the ^{1}A′ State of $HCPN_3^-$, Computed at (U)B3LYP/aug-cc-pVTZ, (14/9)CASPT2/aug-cc-pVTZ, and (U)CCSD(T)/aug-cc-pVTZ Levels of Theory

			(U)B3LYP/aug-cc-pVTZ energies		(14/9)CASPT2/aug-cc-pVTZ energies		(U)CCSD(T)/aug-cc-pVTZ energies	
molecule	electronic state	singly occupied MO	in kcal/mol	in eV	in kcal/mol	in eV	in kcal/mol	in eV
$HCPN_3^-$	^{1}A′ (6π)	none	0 (0)	0 (0)	0	0	0 (0)	0 (0)
$HCPN_3^•$	^{2}A″ (5π)	HOMO	81.7 (80.1)[a]	3.54 (3.47)[a]	86.9	3.77	81.1 (80.2)	3.52 (3.48)
	^{2}A′ (6π)	HOMO−1	81.5 (80.6)	3.53 (3.49)	84.6	3.67	84.8 (83.8)[b]	3.68 (3.64)[b]
	2^{2}A′ (6π)	HOMO−2			98.1[c]	4.25[c]		
	2^{2}A″ (5π)	HOMO−3			108.0[c]	4.68[c]		

[a]UB3LYP predicts an imaginary frequency (i104.6 cm^{-1}) for an out-of-plane vibration of the central N (N2, see Table 1) for the ^{2}A″ state. [b]UCCSD(T) predicts an imaginary frequency (i51.1 cm^{-1}) for an out-of-plane vibration of the central N (N2 in Table 1) for the ^{2}A′ state. [c]The geometry is optimized at the (14/9)CASPT2/aug-cc-pVDZ level.

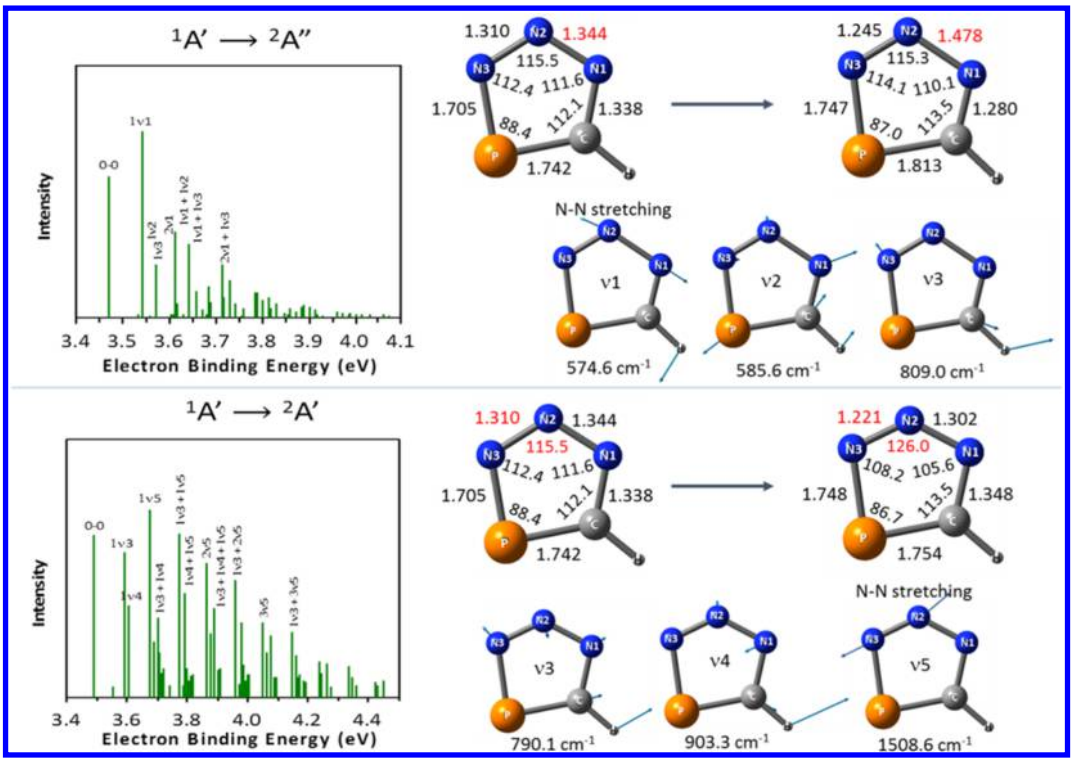

Figure 4. Simulated vibrational progressions (stick spectra) at 20 K for the formation of the two low-lying states of $HCPN_3^•$ from the ^{1}A′ ground state of $HCPN_3^-$, using (U)B3LYP geometries, frequencies, and FCFs. The 0−0 peak for each state is positioned at the (U)B3LYP calculated EA. Geometry changes (the most significant changes are highlighted in red) from the initial state of the anion to the target state of the radical and the active modes (with frequencies) for both transitions are also shown. The assignments of the major peaks in the stick spectra are given.

C−H bond; whereas the π MOs are composed of the out-of-plane 2p AOs of the C and N atoms and the 3p AO of the P atom.

As shown in Figure 3, the HOMO of $HCPN_3^-$ is predicted by B3LYP to be a π MO. It is calculated to be only 0.09 eV above the HOMO−1, which is a σ MO. In $P_2N_3^-$, the energy ordering is opposite. The HOMO is a σ MO; the HOMO−1 is a π MO; and the energy difference between the HOMO and the HOMO−1 (0.56 eV) is much larger in $P_2N_3^-$ than in $HCPN_3^-$. In $(CH)_2N_3^-$ the HOMO is a π MO and the HOMO−1 is a σ MO, as in $HCPN_3^-$, but the energy difference between the HOMO and HOMO−1 (0.33 eV) is also much larger in $(CH)_2N_3^-$ than in $HCPN_3^-$. The MOs of $(CH)_2N_3^-$, $HCPN_3^-$, $P_2N_3^-$, and the correlations among them can be found in Figure S3 in the Supporting Information.

On the basis of the small difference between the B3LYP energies of the HOMO and HOMO−1 of $HCPN_3^-$, one would expect that the IE of an electron from each of these two MOs should be very similar. Therefore, the two lowest states of neutral $HCPN_3^•$—the ^{2}A″ state in which the unpaired electron occupies a π MO and the ^{2}A′ state in which the unpaired electron occupies a σ MO—are likely to be very close in energy.

Table 2 shows the energies of four electronic states of $HCPN_3^•$, relative to the ^{1}A′ ground state of $HCPN_3^-$. These are, by definition, the EAs of the lowest energy electronic states of $HCPN_3^•$. The MOs of $HCPN_3^-$ in Figure 3, from which the singly occupied MOs in the radical originate, are indicated in Table 2.

The ^{2}A″ and the ^{2}A′ states of $HCPN_3$ have almost the same energies (within 0.02 eV) at the UB3LYP/aug-cc-pVTZ level of

DOI: 10.1021/acs.jpca.6b06343
J. Phys. Chem. A XXXX, XXX, XXX−XXX

theory. The CASPT2/aug-cc-pVTZ calculations favor the ^{2}A′ state by 2.3 kcal/mol (0.10 eV). However, at the UCCSD(T)/aug-cc-pVTZ level, the ^{2}A″ state is predicted to be the ground state and to be 3.7 kcal/mol (0.16 eV) lower than the ^{2}A′ state. Although these methods do not agree on whether the unpaired electron occupies a σ or a π MO in the ground state of $HCPN_3^{\bullet}$, the methods do agree that the ^{2}A″ and ^{2}A′ states are close in energy and that the EA of the ground state of the radical is 3.5−3.8 eV. The EA computed for the ground state of the radical is in very good agreement with the experimental value of EA = 3.555 ± 0.010 eV.

Of the ^{2}A″ and ^{2}A′ states, the one with the higher electronic energy is calculated, by the UB3LYP and UCCSD(T) methods, to have an imaginary frequency, corresponding to an out-of-plane vibration of the central N atom (footnotes a and b of Table 2). Loss of the symmetry element that distinguishes between σ and π states means that a geometry optimization that begins on the potential energy surface for the excited state continues on the potential energy surface for the ground state after such a symmetry-breaking molecular distortion.

We also performed CASPT2 calculations on the second lowest ^{2}A′ and ^{2}A″ states of $HCPN_3^{\bullet}$. As shown in Table 2, the calculations show that the unpaired electron in the 2^2A′ and 2^2A″ states occupies a MO that originates from, respectively, HOMO−2 and HOMO−3 of $HCPN_3^-$. The 2^2A′ and 2^2A″ states are much higher in energy than the lowest ^{2}A′ and ^{2}A″ states, and they are likely to be responsible for the spectral features in the higher EBE region (4.2−5.2 eV) in the 193 nm NIPE spectrum in Figure 2.

4.3. Simulation of the Vibrational Progressions in the NIPE Spectra. A potentially useful method for determining whether the ground state of $HCPN_3^{\bullet}$ is ^{2}A′ or ^{2}A″ is to simulate the NIPE spectra for formation of each of these states from the ^{1}A′ state of $HCPN_3^-$ and to see which of these simulations provides a better fit to the low energy region of the experimental NIPE spectrum. We simulated the vibrational progressions in the transition from the ^{1}A′ ground state of $HCPN_3^-$ to each of the two lowest-lying electronic states of $HCPN_3^{\bullet}$ (^{2}A″ and ^{2}A′), based on the calculated Franck−Condon factors (FCFs) for different vibrations in each of these two transitions.

Figure 4 shows the vibrational progressions, simulated using the (U)B3LYP geometries, frequencies, and FCFs. The geometry changes and the active vibrational modes that yield the vibrational progressions for each transition are also shown in Figure 4. Simulations using (U)CCSD(T) geometries, frequencies, and FCFs gave vibrational progression patterns that are very similar to (U)B3LYP; and the (U)CCSD(T) stick spectra are provided in Figure S4 of the Supporting Information.

As shown in Figure 4, the electronic transitions from the ^{1}A′ ground state of $HCPN_3^-$ to the two low-lying states of $HCPN_3^{\bullet}$ both feature relatively strong 0−0 peaks and long vibrational progressions. The vibrational progressions associated with the ^{2}A′ state are more complex and attenuate less slowly than those associated with the ^{2}A″ state. The long vibrational progressions for both states are due to significant geometry changes from the anion to the radical. These geometry changes can be understood based on the MOs in Figure 3.

For example, in the ^{1}A′ → ^{2}A″ transition (Figure 4), an electron is removed from the B3LYP HOMO, which is a π MO, of $HCPN_3^-$. As shown in Figure 3, this MO is π bonding between three pairs of nearest-neighbor atoms (N1−N2, N3−P, and P−C), but π antibonding between the N2−N3 and N1−C bonds. Removing one electron from this orbital should lead to lengthening of the N1−N2, N3−P, and P−C bonds, and shortening of the N2−N3 and N1−C bonds, which is found to be the case when the calculated geometries of the ^{1}A′ and ^{2}A″ states are compared. The most significant geometrical change is the lengthening of the N1−N2 bond, from 1.344 to 1.478 Å.

One quantum of the N1−N2 stretching vibration (υ_1 = 574.6 cm^{-1}), which is associated with this geometry change, is calculated to give rise to the strongest peak in the simulated spectrum for the ^{1}A′ → ^{2}A″ transition. The other two active modes in the ^{1}A′ → ^{2}A″ transition are υ_2 = 585.6 and υ_3 = 809.0 cm^{-1}. The motions of the atoms in each of these vibrations are shown in Figure 4.

In the ^{1}A′ → ^{2}A′ transition, the electron is detached from HOMO−1 in Figure 3, which is a σ MO and mainly N2−N3 antibonding. Therefore, there is a shortening of the N2−N3 bond distance, from 1.310 to 1.221 Å, associated with this transition.

Consequently, long and strong vibrational progressions due to N2−N3 stretching (υ_5 = 1508.6 cm^{-1}) appear in the simulation. In fact, the most intense peak in the simulation is due to one quantum of the N2−N3 stretching vibration. Two more vibrations, υ_3 = 790.1 and υ_4 = 903.3 cm^{-1} are also calculated to be active in the ^{1}A′ → ^{2}A′ transition. The motions of the atoms in each of these vibrations are depicted in Figure 4.

The spacing between the first two peaks in the 266 nm spectrum is 85 meV = 685 cm^{-1}; whereas, the calculated spacings between the first two major peaks in the simulated spectra are, respectively, 574.6 cm^{-1} for ^{2}A″ and 790.1 cm^{-1} for 2A′. Therefore, the simulated spectrum for neither ^{2}A″ nor ^{2}A′ provides a good fit to the separation between the first two peaks in the 266 nm spectrum.

However, the average of the spacing between the first two peaks in the two states [(574 + 790)/2 = 682 cm^{-1}] matches the experimental value reasonably well. This suggests that the first two peaks in the 266 nm experimental spectrum may both have contributions from the first two peaks for both the ^{2}A″ and ^{2}A′ states, but this would be the case only if the 0−0 peaks for both states appear at almost the same energy.

4.4. Simulation of the NIPE Spectra of $HCPN_3^-$. We simulated the experimental 266 nm NIPE spectrum of $HCPN_3^-$ by convoluting the (U)B3LYP calculated stick spectrum with Gaussian functions having full widths of 45 meV at half maxima for each stick. As shown in Figure 5a and b, after small adjustments of the (U)B3LYP calculated energies of the 0−0 bands for the two lowest electronic states of $HCPN_3^{\bullet}$ (+0.09 eV for ^{2}A″ and +0.07 eV for ^{2}A′, which yield EA = 3.56 eV for both the ^{2}A″ and ^{2}A′ states of $HCPN_3^{\bullet}$), the peak positions in the simulated NIPE spectrum of $HCPN_3^-$ match those in the experimental 266 nm spectrum reasonably well.

Alternatively, we found that if we adjust the 0−0 bands for ^{2}A″ and ^{2}A′ states by +0.09 and +0.11 eV, respectively, the simulated (U)B3LYP NIPE spectrum matches the experimental 266 nm spectrum reasonably well in terms of the peak intensities, but slightly less well in terms of peak positions. (Figure S5 in the Supporting Information) This latter pair of adjustments yields EA = 3.56 eV for the ^{2}A″ state and EA = 3.60 eV for the ^{2}A′ state of $HCPN_3^{\bullet}$.

DOI: 10.1021/acs.jpca.6b06343
J. Phys. Chem. A XXXX, XXX, XXX−XXX

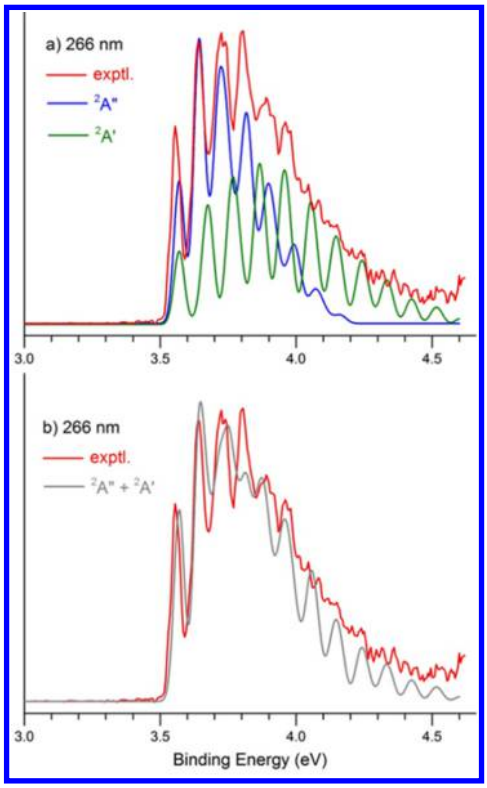

Figure 5. (a) Convoluted spectra (Gaussian line shapes with 45 meV full widths at half maxima), using the (U)B3LYP/aug-cc-pVTZ stick spectra, for the $^2A''$ (in blue) and $^2A'$ (in green) states of $HCPN_3^{\bullet}$, superimposed onto the experimental 266 nm NIPE spectrum (red) of $HCPN_3^-$. The (U)B3LYP predicted 0−0 band positions of $^2A''$ and $^2A'$ have been slightly adjusted, by +0.09 (3.47 → 3.56 eV) for $^2A''$ and by +0.07 eV (3.49 → 3.56 eV) for $^2A'$; (b) The spectrum with contributions from the $^2A''$ and $^2A'$ states summed (in gray), superimposed on the experimental 266 nm spectrum (in red).

We have also simulated the 266 nm NIPE spectra of $HCPN_3^-$ with other possible adjustments of the calculated energies of the 0−0 bands of $^2A'$ and $^2A''$. In one simulation, we placed the 0−0 band of the $^2A'$ state 0.1 eV higher than that of the $^2A''$ state; in another simulation we placed the 0−0 peak of $^2A'$ at an energy lower than that of $^2A''$, thus assuming that $^2A'$ is the ground state of $HCPN_3^{\bullet}$. These additional simulations are presented in Figures S6 and S7 of the Supporting Information. However, these simulated spectra agree less well with the experimental 266 nm NIPE spectrum than the simulated spectra in Figures 5 and S5 do. Therefore, we tentatively assign the $^2A''$ state, in which the unpaired electron occupies a π MO, as the ground state of $HCPN_3^{\bullet}$, but with the $^2A'$ σ state being nearly degenerate and higher in energy by less than ~1.0 kcal/mol.[36]

It is worth mentioning that starting with EBE > 4.0 eV, the bands in the 266 nm experimental NIPE spectrum seem to sit on top of a background, which makes the spectral features in this region appear more intense than they would be if only direct detachment processes were involved. Resonant photodetachment[37] via some excited state of $HCPN_3^-$, may give rise to an underlying band in this region, which could account for the differences between the experimental and simulated NIPE spectra at EBE > 4.0 eV. Resonant photodetachment was also suggested to occur in our previous NIPES studies of the 1,2,4,5-tetraoxatetramethylenebenzene (TOTMB) radical anion[38] and $P_2N_3^-$.[20]

5. CONCLUSIONS

B3LYP calculations find that the two highest occupied MOs of $HCPN_3^-$, a σ MO and a π MO, have very similar orbital energies. This near energetic degeneracy of two occupied MOs leads to the expectation that the $^2A'$ σ and $^2A''$ π states of the $HCPN_3^{\bullet}$ radical are close in energy. This conjecture is supported by the results of (U)B3LYP, CASPT2, and (U)CCSD(T) calculations, which all find that these two electronic states of the radical do, indeed, have very similar energies.

We have calculated the FCFs for the vibrations associated with both a $^1A' \rightarrow {}^2A'$ and a $^1A' \rightarrow {}^2A''$ transition in the NIPE spectrum of $HCPN_3^-$, and we have used the computed vibrational progressions to simulate the NIPE spectrum. The best fit to the experimental spectrum is obtained when the $^2A''$ π state is assumed to be equal to or 1.0 kcal/mol lower than the energy of the $^2A'$ σ state in the $HCPN_3^{\bullet}$ radical that is formed by photodetachment of an electron from $HCPN_3^-$. This assignment contrasts with our recent finding that the ground state of $P_2N_3^{\bullet}$ is a 6π-electron, σ radical state.[20]

■ ASSOCIATED CONTENT

Supporting Information

The Supporting Information is available free of charge on the ACS Publications website at DOI: 10.1021/acs.jpca.6b06343.

Mass spectrum of $HCPN_3^-$ (Figure S1), the 20 K NIPE spectrum of $(CH)_2N_3^-$ at 266 nm (4.661 eV) (Figure S2), the MOs of $(CH)_2N_3^-$, $HCPN_3^-$, $P_2N_3^-$, and the correlations among them (Figure S3), comparison of B3LYP and CCSD(T) simulations of vibrational progressions (Figure S4), additional simulations of the NIPE spectra by adjusting the calculated 0−0 band positions for each electronic state relative to the experiments (Figures S5−S7), the simulated 266 nm spectra with Gaussian functions of 50 and 40 meV full widths at half maxima (Figures S8 and S9), and coordinates and energies of calculated structures (Table S1); computed Franck−Condon factors (Table S2) (PDF)

■ AUTHOR INFORMATION

Corresponding Authors

*(W.T.B.) E-mail: borden@unt.edu. Telephone: 1-940-565-3658.

*(C.C.C.) E-mail: ccummins@mit.edu. Telephone: 1-617-253-5332.

*(B.C.) E-mail: cberic@hotmail.com. Telephone: 1-940-312-9354.

*(X.-B.W.) E-mail: xuebin.wang@pnnl.gov. Telephone: 1-509-371-6132.

Notes

The authors declare no competing financial interest.

■ ACKNOWLEDGMENTS

The NIPES research done at PNNL was supported by U.S. Department of Energy (DOE), Office of Science, Office of Basic Energy Sciences, the Division of Chemical Sciences, Geosciences, and Biosciences, and performed using EMSL, a national scientific user facility sponsored by DOE's Office of

DOI: 10.1021/acs.jpca.6b06343
J. Phys. Chem. A XXXX, XXX, XXX−XXX

Biological and Environmental Research and located at Pacific Northwest National Laboratory, which is operated by Battelle Memorial Institute for the DOE. The theoretical calculations at UNT were supported by Grant B0027 from the Robert A. Welch Foundation. The synthesis work of [TBA][$HCPN_3$] was supported by the National Science Foundation under Grant No. CHE-1362118. G.-L.H. thanks Dr. Shaoguang Zhang from PNNL for providing the dry and degassed acetonitrile.

REFERENCES

(1) Engelking, P. C.; Lineberger, W. C. Laser Photoelectron Spectrometry of $C_5H_5^-$: A Determination of the Electron Affinity and Jahn-Teller Coupling in Cyclopentadienyl. *J. Chem. Phys.* **1977**, *67*, 1412−1417.

(2) Ichino, T.; Wren, S. W.; Vogelhuber, K. M.; Gianola, A. J.; Lineberger, W. C.; Stanton, J. F. The Vibronic Level Structure of the Cyclopentadienyl Radical. *J. Chem. Phys.* **2008**, *129*, 084310.

(3) Applegate, B. E.; Miller, T. A.; Barckholtz, T. A. The Jahn−Teller and Related Effects in the Cyclopentadienyl Radical. I. The *ab initio* Calculation of Spectroscopically Observable Parameters. *J. Chem. Phys.* **2001**, *114*, 4855−4868.

(4) Applegate, B. E.; Bezant, A. J.; Miller, T. A. The Jahn−Teller and Related Effects in the Cyclopentadienyl Radical. II. Vibrational Analysis of the $\tilde{A}^2A_2''$-$\tilde{X}^2E_1''$ Electronic Transition. *J. Chem. Phys.* **2001**, *114*, 4869−4882.

(5) Borden, W. T.; Davidson, E. R. Potential Surfaces for the Planar Cyclopentadienyl Radical and Cation. *J. Am. Chem. Soc.* **1979**, *101*, 3771−3775.

(6) Zhou, X.; Hrovat, D. A.; Borden, W. T. Calculations of the Effects of Substituents on Bond Localization in Annelated Cyclopentadienyl Radicals. *J. Am. Chem. Soc.* **2007**, *129*, 10785−10794.

(7) Baudler, M.; Düster, D.; Ouzounis, D. Beiträge zur Chemie des Phosphors. 172. Existenz und Charakterisierung des Pentaphosphacyclopentadienid-Anions, P_5^-, des Tetraphosphacyclopentadienid-Ions, P_4CH^-, und des Triphosphacyclobutenid-Ions, $P_3CH_2^-$. *Z. Anorg. Allg. Chem.* **1987**, *544*, 87−94.

(8) Baudler, M.; Akpapoglou, S.; Ouzounis, D.; Wasgestian, F.; Meinigke, B.; Budzikiewicz, H.; Münster, H. On the Pentaphosphacyclopentadienide Ion, P_5^-. *Angew. Chem., Int. Ed. Engl.* **1988**, *27*, 280−281.

(9) Grützmacher, H. The Power of Experiment and Imagination: The Discovery of Pentaphosphacyclopentadienide, $[P_5]^-$. *Z. Anorg. Allg. Chem.* **2012**, *638*, 1877−1879.

(10) Vij, A.; Pavlovich, J. G.; Wilson, W. W.; Vij, V.; Christe, K. O. Experimental Detection of the Pentaazacyclopentadienide (Pentazolate) Anion, *cyclo*-N_5^-. *Angew. Chem.* **2002**, *114*, 3177−3180.

(11) Nguyen, M. T. Polynitrogen Compounds: 1. Structure and Stability of N_4 and N_5 Systems. *Coord. Chem. Rev.* **2003**, *244*, 93−113.

(12) Geiger, U.; Haas, Y. Preparation of the Cyclopentazole Anion in the Bulk: A Computational Study. *J. Phys. Chem. B* **2016**, *120*, 6208−6214.

(13) Velian, A.; Cummins, C. C. Synthesis and Characterization of $P_2N_3^-$: An Aromatic Ion Composed of Phosphorus and Nitrogen. *Science* **2015**, *348*, 1001−1004.

(14) Hering-Junghans, C.; Rivard, E. Accessing an Aromatic Diphosphatriazolate Anion by Formal Inorganic "Click" Chemistry. *Angew. Chem., Int. Ed.* **2015**, *54*, 10077−10079.

(15) Jin, Y.; Perera, A.; Bartlett, R. J. Spectroscopic Analysis of Diphosphatriazolate Pnion ($P_2N_3^-$) by Coupled-cluster Methods as a Step Toward N_5^-. *Chem. Phys. Lett.* **2015**, *640*, 68−71.

(16) Mandal, S.; Nandi, S.; Anoop, A.; Chattaraj, P. K. Viability of Aromatic All-Pnictogen Anions. *Phys. Chem. Chem. Phys.* **2016**, *18*, 11738−11745.

(17) Nizovtsev, A. S. Search for Aromatic Anions in the $P_2E_3^-$ (E = N, P, As, Sb, Bi) Series. *Phys. Chem. Chem. Phys.* **2016**, *18*, 16084−16087.

(18) Ichino, T.; Andrews, D. H.; Rathbone, G. J.; Misaizu, F.; Calvi, R. M. D.; Wren, S. W.; Kato, S.; Bierbaum, V. M.; Lineberger, W. C. Ion Chemistry of 1H-1,2,3-Triazole. *J. Phys. Chem. B* **2008**, *112*, 545−557.

(19) Dillon, J.; Yarkony, D. R.; Schuurman, M. S. On the Simulation of Photoelectron Spectra Complicated by Conical Intersections: Higher-order Effects and Hot Bands in the Photoelectron Spectrum of Triazolide $(CH)_2N_3^-$. *J. Chem. Phys.* **2011**, *134*, 184314.

(20) Hou, G.-L.; Chen, B.; Transue, W. J.; Hrovat, D. A.; Cummins, C. C.; Borden, W. T.; Wang, X.-B. Negative Ion Photoelectron Spectroscopy of $P_2N_3^-$: Electron Affinity and Electronic Structures of $P_2N_3^{\bullet}$. *Chem. Sci.* **2016**, *7*, 4667−4675.

(21) Gianola, A. J.; Ichino, T.; Hoenigman, R. L.; Kato, S.; Bierbaum, V. M.; Lineberger, W. C. Thermochemistry and Electronic Structure of the Pyrrolyl Radical. *J. Phys. Chem. A* **2004**, *108*, 10326−10335.

(22) Gianola, A. J.; Ichino, T.; Hoenigman, R. L.; Kato, S.; Bierbaum, V. M.; Lineberger, W. C. Photoelectron Spectra and Ion Chemistry of Imidazolide. *J. Phys. Chem. A* **2005**, *109*, 11504−11514.

(23) Gianola, A. J.; Ichino, T.; Kato, S.; Bierbaum, V. M.; Lineberger, W. C. Thermochemical Studies of Pyrazolide. *J. Phys. Chem. A* **2006**, *110*, 8457−8466.

(24) Transue, W. J.; Velian, A.; Nava, M.; Martin-Drumel, M. A.; Womack, C. C.; Jiang, J.; Hou, G.-L.; Wang, X.-B.; McCarthy, M. C.; Field, R. W.; Cummins, C. C. A Molecular Precursor to Phosphaethyne and its Application in Synthesis of the Aromatic 1,2,3,4-Phosphatriazolate Anion. *J. Am. Chem. Soc.* **2016**, *138*, 6731−6734.

(25) Wang, X.-B.; Wang, L.-S. Development of a Low-temperature Photoelectron Spectroscopy Instrument Using an Electrospray Ion Source and a Cryogenically Controlled Ion Trap. *Rev. Sci. Instrum.* **2008**, *79*, 073108.

(26) B3LYP is a combination of Becke's 3-parameter hybrid exchange functional Becke, A. D. *J. Chem. Phys.* **1993**, *98*, 5648. with the electron correlation functional in Lee, C.; Yang, W.; Parr, R. G. *Phys. Rev. B: Condens. Matter Mater. Phys.* **1988**, *37*, 785.

(27) Andersson, K.; Malmqvist, P. Å.; Roos, B. O. Second-order Perturbation Theory with a Complete Active Space Self-consistent Field Reference Function. *J. Chem. Phys.* **1992**, *96*, 1218−1226.

(28) Purvis, G. D.; Bartlett, R. J. A Full Coupled-cluster Singles and Doubles Model: The Inclusion of Disconnected Triples. *J. Chem. Phys.* **1982**, *76*, 1910−1918.

(29) Raghavachari, K.; Trucks, G. W.; Pople, J. A.; Head-Gordon, M. A Fifth-order Perturbation Comparison of Electron Correlation Theories. *Chem. Phys. Lett.* **1989**, *157*, 479−483.

(30) Dunning, T. H. Gaussian Basis Sets for Use in Correlated Molecular Calculations. I. The Atoms Boron through Neon and Hydrogen. *J. Chem. Phys.* **1989**, *90*, 1007−1023.

(31) Kendall, R. A.; Dunning, T. H.; Harrison, R. J. Electron Affinities of the First-row Atoms Revisited. Systematic Basis Sets and Wave Functions. *J. Chem. Phys.* **1992**, *96*, 6796−6806.

(32) Frisch, M. J.; Trucks, G. W.; Schlegel, H. B.; Scuseria, G. E.; Robb, M. A.; Cheeseman, J. R.; Scalmani, G.; Barone, V.; Mennucci, B.; Petersson, G. A., et al. *Gaussian 09*, Revision D.01; Gaussian, Inc: Wallingford, CT, 2013.

(33) Aquilante, F.; Autschbach, J.; Carlson, R. K.; Chibotaru, L. F.; Delcey, M. G.; De Vico, L.; Galván, I. F.; Ferré, N.; Frutos, L. M.; Gagliardi, L.; et al. MOLCAS 8: New Capabilities for Multiconfigurational Quantum Chemical Calculations Across the Periodic Table. *J. Comput. Chem.* **2016**, *37*, 506−541.

(34) Werner, H.-J.; Knowles, P. J.; Knizia, G.; Manby, F. R.; Schütz, M.; Celani, P.; Korona, T.; Lindh, R.; Mitrushenkov, A.; Rauhut, G., et al. *MOLPRO*, version 2010.1, A Package of *Ab initio* Programs, see http://www.molpro.net (accessed December 10, 2015).

(35) Mozhayskiy, V. A.; Krylov, A. I. *ezSpectrum*, version 3.0; see http://iopenshell.usc.edu/downloads (accessed December 10, 2015).

(36) Simulations using (U)CCSD(T) geometries, frequencies and FCFs gave similar vibrational patterns to the (U)B3LYP simulations in Figure 5. The (U)CCSD(T) stick spectra are provided in Figure S4. In addition, we also simulated two sets of 266 nm spectra, by convoluting the (U)B3LYP calculated stick spectrum with Gaussian functions having full widths of 40 and 50 meV at half maxima for each stick,

DOI: 10.1021/acs.jpca.6b06343
J. Phys. Chem. A XXXX, XXX, XXX−XXX

respectively, to account for the variation of energy resolution of our TOF type photoelectron spectrometer in the observed photoelectron energy range (EBE = 3.5−4.3 eV). These two simulated spectra (Figures S8 and S9) gave similar fits to the experimental spectrum as the simulated spectra with the 45 meV energy resolution in Figure 5.

(37) Schiedt, J.; Weinkauf, R. Resonant Photodetachment via Shape and Feshbach Resonances: *p*-Benzoquinone Anions as a Model System. *J. Chem. Phys.* **1999**, *110*, 304−314.

(38) Hrovat, D. A.; Hou, G.-L.; Wang, X.-B.; Borden, W. T. Negative Ion Photoelectron Spectroscopy Confirms the Prediction that 1,2,4,5-Tetraoxatetramethylenebenzene Has a Singlet Ground State. *J. Am. Chem. Soc.* **2015**, *137*, 9094−9099.

DOI: 10.1021/acs.jpca.6b06343
J. Phys. Chem. A XXXX, XXX, XXX−XXX